OPEN ACCESS
Journal of Innovative Optical Health Sciences
Vol. 16, No. 5 (2023) 2350007 (8 pages)

DOI: 10.1142/S1793545823500074

World Scientific
www.worldscientific.com

# Optical second-harmonic generation imaging for identifying gastrointestinal stromal tumors

Shichao Zhang*, Xingxin Huang*, Deyong Kang†, Jikui Miao*, Zhenlin Zhan*, Guoxian Guan‡, Jianxin Chen*, Yongjian Zhou§,¶,** and Lianhuang Li*,‖,**

*Key Laboratory of OptoElectronic Science and Technology for Medicine of Ministry of Education
Fujian Provincial Key Laboratory for Photonics Technology
Fujian Normal University, Fuzhou 350007, P. R. China

†Department of Pathology
Fujian Medical University Union Hospital
Fuzhou 350001, P. R. China

‡Department of Colorectal Surgery
The First Affiliated Hospital of Fujian Medical University
Fuzhou 350001, P. R. China

§Department of Gastric Surgery
Fujian Medical University Union Hospital
Fuzhou 350001, P. R. China
¶zhouyjbju@163.com
‖lhli@fjnu.edu.cn

Received 9 November 2022
Revised 13 March 2023
Accepted 13 March 2023
Published 6 May 2023

Gastrointestinal stromal tumors (GISTs) are the most common mesenchymal tumors arising in the digest tract. It brings a challenge to diagnosis because it is asymptomatic clinically. It is well known that tumor development is often accompanied by the changes in the morphology of collagen fibers. Nowadays, an emerging optical imaging technique, second-harmonic generation (SHG), can directly identify collagen fibers without staining due to its noncentrosymmetric properties. Therefore, in this study, we attempt to assess the feasibility of SHG imaging for detecting GISTs by monitoring the morphological changes of collagen fibers in tumor microenvironment. We found that collagen alterations occurred obviously in the GISTs by comparing with normal tissues, and furthermore, two morphological features from SHG images were extracted to quantitatively assess the morphological difference of collagen fibers between normal

**Corresponding authors.

muscular layer and GISTs by means of automated image analysis. Quantitative analyses show a significant difference in the two collagen features. This study demonstrates the potential of SHG imaging as an adjunctive diagnostic tool for label-free identification of GISTs.

*Keywords*: Multiphoton imaging; two-photon excited fluorescence; second-harmonic generation; gastrointestinal stromal tumors.

## 1. Introduction

Although gastrointestinal stromal tumors (GISTs) are rare gastrointestinal neoplasms, they represent the most common mesenchymal tumor arising in the digest tract.[1,2] GISTs usually originate in the muscular layer of the gastrointestinal tract.[3] With the development of endoscopy technology, the detection rate of small GISTs began to increase, greatly improving the prognosis of patients.[4,5] Histological diagnosis of biopsy specimens and surgical specimens is the gold standard for the diagnosis of GISTs, but this method requires a series of tedious operations such as fixation, embedding, and staining. Therefore, the development of a new imaging technology for label-free detection of GISTs may have important clinical significance.

It is reported that GISTs would cause collagen deposition due to desmoplastic reaction which refers to a cellular host response and is the result of an increased synthesis of extracellular matrix (ECM) proteins (mainly collagen) by stromal cells such as myofibroblasts.[6–8] Desmoplastic tissues are characterized by the presence of an abundant collagen-rich ECM with cells, mainly fibroblasts and myofibroblasts. However, it is difficult to accurately identify collagen changes in H&E-stained images. Second-harmonic generation (SHG) imaging can clearly identify collagen fibers in extracellular matrix due to its noncentrosymmetric structure.[9,10] Another nonlinear optical technology, namely two-photon excited fluorescence (TPEF) imaging, can help us to recognize cellular structures due to endogenous fluorescence molecules such as the flavin adenine dinucleotide (FAD), nicotinamide adenine dinucleotide (NADH) or nicotinamide adenine dinucleotide phosphate (NADPH), and so on.[11,12] Moreover, elastin can also produce TPEF signal which could help us identify elastic fibers and blood vessel. Multiphoton microscopy (MPM) combining SHG and TPEF imaging has been widely used for researching precancerous gastric lesions and gastric cancer, and revealed collagen variations in diseased tissues.[13–16] It can be seen that collagen morphology in gastric tissues would change with the progression of diseases, and thus detecting collagen feature changes through SHG image would provide us a way to distinguish normal from abnormal gastric tissues. Therefore, in this study, we attempt to identify GISTs by SHG imaging, and furthermore, in order to quantify the morphological difference of collage fibers between normal gastric tissue and GISTs, the aspect ratio (AR) and correlation is extracted from SHG images.

## 2. Materials and Methods

### 2.1. *Sample preparation*

This study was conducted with approval from the Institutional Review Board of the Fujian Medical University Union Hospital. Before participating in the study, each patient signed an informed consent. In this work, 20 fresh gastric specimens were collected from 20 patients undergoing surgery, including 10 cases of normal gastric tissues and 10 cases of gastrointestinal stromal tumor tissues, and the age and gender of patients were presented in Table 1. Each sample was sectioned longitudinally by a cryostat microtome (Thermo Scientific CryoStar NX50, USA) and two consecutive slices

Table 1. The basic information of patients.

| Normal samples | | | Gastric GISTs | | |
|---|---|---|---|---|---|
| Patient no. | Gender | Age | Patient no. | Gender | Age |
| 1 | male | 67 | 1 | male | 52 |
| 2 | male | 56 | 2 | male | 49 |
| 3 | male | 66 | 3 | male | 38 |
| 4 | male | 79 | 4 | male | 65 |
| 5 | male | 49 | 5 | male | 81 |
| 6 | male | 58 | 6 | female | 47 |
| 7 | female | 69 | 7 | female | 44 |
| 8 | female | 62 | 8 | female | 76 |
| 9 | female | 51 | 9 | female | 71 |
| 10 | female | 75 | 10 | female | 55 |

with 10 $\mu$m in thickness were obtained. Thereinto, one section was used for multiphoton imaging and the other was stained with H&E for comparative analysis. In the course of experiment, we dripped small amounts of phosphate-buffered saline (PBS) on the slices in order to prevent dehydration or shrinkage and then placed a coverslip to allow multiphoton imaging with oil.

### 2.2. *Multiphoton microscope*

We used a commercial microscope (LSM 880, Zeiss, Germany) which was combined with a mold-locked femtosecond Ti:sapphire laser (Chamelcon Ultra, Coherent, USA) to perform multiphoton imaging. The 810 nm wavelength was selected as excitation light in the experiment to generate TPEF and SHG signals, and an oil immersion objective (Plan-Apochromat 63×, NA = 1.4, Zeiss, German) was selected to obtain high-resolution images. The backscattered intrinsic TPEF and SHG signals were received in two-track channel mode, where SHG signal in the wavelength range of 395–415 nm were collected by a GaAsP photomultiplier tube (PMT), and TPEF signal in the wavelength range of 430–759 nm were detected using a 32-channel GaAsP PMT array detector. To increase contrast, TPEF images were labeled by pseudo-colored red and SHG images are labeled by pseudo-colored green. Additionally, all the H&E-stained slices were reviewed by a certified pathologist, and then were scanned by a commercial whole slide scanner (VM1000, Motic, China). In this work, all the MPM images were compared with the corresponding H&E-stained images to verify the accuracy of multiphoton imaging.

### 2.3. *Quantification of morphological features*

To test the morphological difference of collagen fibers between normal gastric tissue and GISTs, we measured the AR and correlation value. The AR was defined as the ratio of the minor axis to the primary axis of the fitted circle on the thresholded two-dimensional discrete Fourier Transform (2D DFT) image.[17,18] We usually used it to evaluate the degree of disorganization of collagen fibers, thereinto, when the AR value is close to zero, the collagen fibers are more anisotropic, and if the AR value is close to one, the collagen fibers are more isotropic.

We also used the gray-level co-occurrence matrix (GLCM) methods to measure the correlation of collagen fibers which is a measurement of intensity correlation as a function of pixel distance.[19,20] The downward trend of correlation is related to collagen fibers structure. In detail, if collagen fibers are distinct and linear, the correlation value declines quickly at first as the pixel distance increases, and if collagen fibers loss its linear structrue, the decline of correlation is slower compared to the neat collagen fibers.[21] To give a more intuitive representation of this downward trend in collagen structure caused by the morphological difference between abnormal and normal tissues, the pixel distance where the correlation falls to 0.5 was measured as a characteristic parameter to assess the difference.

In this work, we used the Opencv library and Scikit-Image library of Python language to calculate AR and correlation value. All statistical analyses were performed using GraphPad Prism 8.0.2. Quantitative results are expressed as mean and standard deviation (mean ± SD). Statistical differences are determined using Mann–Whitney $U$ test, and $P < 0.05$ is considered to be statistical difference.

## 3. Results

### 3.1. *SHG imaging of normal and abnormal gastric tissues*

First, we performed SHG imaging of healthy tissues by biomedical MPM for comparative analysis. MPM images of mucosal layer from a frozen section are presented in Figs. 1(a) and 1(b), and those of submucosal layer from another slice are shown in Figs. 1(d) and 1(e). SHG images present that collagen distributions in mucosa (Fig. 1(a)) and submucosa (Fig. 1(d)) are different. Collagen fibers in the mucosal layer are sparse and form a circle (yellow arrows in Fig. 1(a)) called basement membrane, while the submucosa is mainly composed of collagen fibers. These microstructural features can not to be directly observed by H&E-stained image. Combining with TPEF imaging, we can further recognize normal gastric glands (cyan arrows in Fig. 1(b)) surrounded by the collagen fibers in the mucosa and blood vessel (white arrow in Fig. 1(e)) in the submucosa, which are consistent with the corresponding H&E-stained images (Figs. 1(c) and 1(f)).

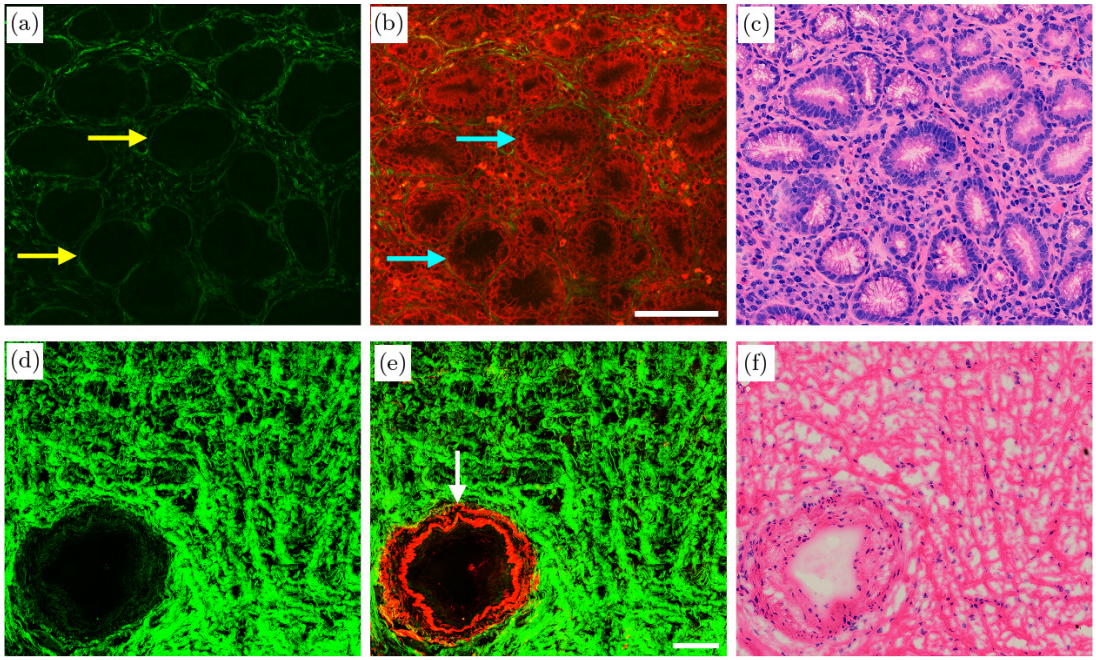


Fig. 1. MPM images of normal mucosal and submucosal layers and corresponding H&E-stained images. (a, d) SHG images; (b, e) Overlaid SHG and TPEF signal; (c, f) H&E-stained images. Yellow arrows: Basement membrane; cyan arrows: Gastric glands; white arrow: Blood vessel. Scale bar: 100 $\mu$m.

Figure 2 shows the MPM images of normal gastric muscularis and corresponding H&E-stained image. SHG imaging reveals that there are some collagen fibers in muscular layer and these fibers are parallel as shown in Figs. 2(a) and 2(d). The elongated collagen structures in the SHG image seem to outline cellular structure and may be used to separate muscular cells or interstitial cells. By the combination with TPEF imaging, we can also observe some elastic fibers displayed in Figs. 2(b) and 2(e). The composite images is helpful for our understanding of the spatial distribution of tissue components. These structural features are in agreement with that from the corresponding H&E-stained images (Figs. 2(c) and 2(f)). The above results show that MPM has advantages in identifying the microstructure of gastric tissues because collagen fibers and endogenous fluorophores are particularly abundant in biological samples. Thereinto, collagen fibers can generate SHG signal, and elastin in vascular wall as well as FAD and NADH in cells can generate TPEF signal.[22]

Second, we used MPM for imaging GISTs. SHG images demonstrate that collagen fibers in GISTs (Figs. 3(a) and 3(d)) obviously increase due to desmoplastic reaction often caused by tumor invasion, and are chaotic and slender by comparing with normal muscularis (Figs. 2(a) and 2(d)). Combining with TPEF imaging, we can find a small blood vessel (white arrow in Fig. 3(b)) in the tumor, which is confirmed by the corresponding H&E-stained image (Fig. 3(c)) and often regarded as a malignant biological parameter.[23] The experimental results obtained by the SHG imaging reveal that collagen distributions in tumor microenvironment are completely different from normal tissues, and therefore SHG imaging may be used for identifying abnormal tissues.

### 3.2. *Quantitative analysis*

GISTs often occur in the muscular layer at first, and then grow toward the lumen of gastrointestinal tract. Therefore, two morphological feature descriptors including the AR and correlation values are used to measure the collagen morphological changes in tumor microenvironment by comparing with normal muscularis. We randomly chose one region of interest ($500 \times 500$ pixels) in SHG images from each slice for imaging analysis. As shown in Table 2, the mean and SD of AR in the GISTs and normal muscular layer are $0.544 \pm 0.196$ and

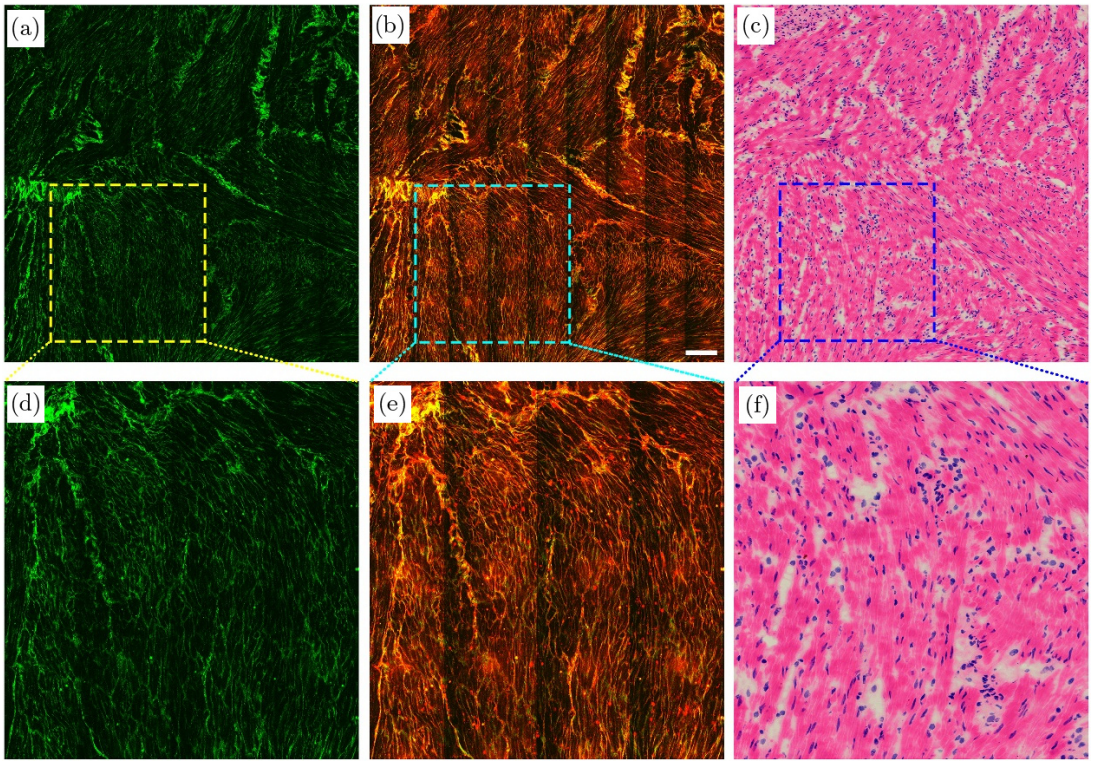


Fig. 2. MPM images of the normal longitudinal muscular layer and corresponding H&E-stained image. (a) SHG image; (b) Overlaid SHG and TPEF signal; (c) H&E-stained image; (d)–(f) Zoom-in images of the boxed regions. Scale bar: 100 $\mu$m.

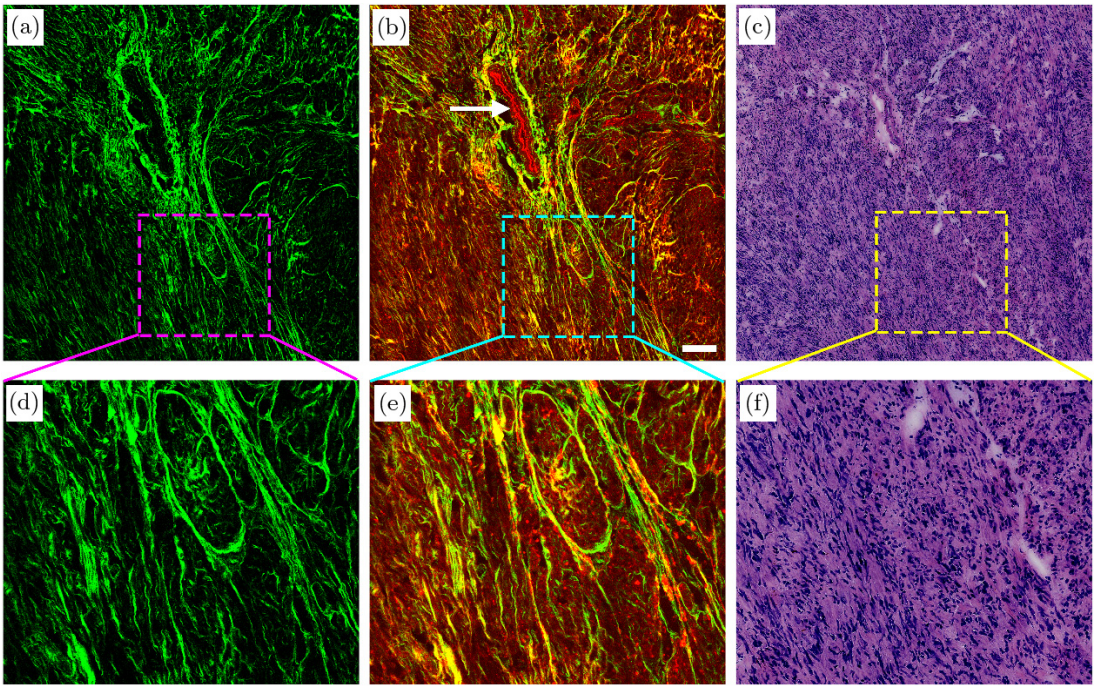


Fig. 3. MPM images of GISTs and corresponding H&E-stained image. (a) SHG image; (b) Overlaid SHG and TPEF signal; (c) H&E-stained image; (d)–(f) Zoom-in images of the boxed regions. White arrow: Blood vessel. Scale bar: 100 $\mu$m.

Table 2. Two characteristic parameters from normal muscularis and GISTs.

| Samples | AR value | Pixel distance |
|---|---|---|
| Normal | 0.318 ± 0.042 | 4.74 ± 1.82 |
| GISTs | 0.544 ± 0.196 | 10.07 ± 5.30 |

$0.318 \pm 0.042$, respectively, reflecting collagen fibers are more chaotic in tumors, and statistical significant difference ($P = 0.003$) is found between the two sets of data.

Figure 4 shows the correlation values as a function of pixel distance from normal muscularis and GISTs, respectively. The correlation of normal muscularis decreases sharply with the increase of distance because of the presence of aligned fibers, while the correlation of GISTs decreases slowly because the regularity in original repetition patterns of collagen fibers is lost. The pixel distance at which the correlation value drops to 0.5 (red line in Fig. 4) is used as a measure of the difference in collagen morphological features between normal muscular layer and GISTs. As shown in Table 2, the pixel distance at the correlation value of 0.5 from the normal muscular layer is $4.74 \pm 1.82$, while from the GISTs is $10.07 \pm 5.30$. Statistical analysis demonstrates that the two sets of data are also different ($P = 0.029$). These data indicate that these feature descriptors might help recognize abnormal tissues and may be used as biomarkers to monitor collagen changes in tumor microenvironment.

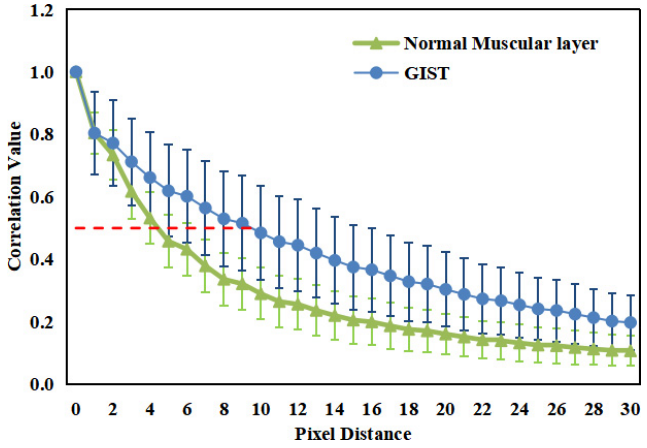


Fig. 4. Correlation as a function of pixel distance from normal muscular layer and GISTs, respectively. Error bars indicate standard deviations.

## 4. Discussion

GISTs are the most common mesenchymal tumors of the gastrointestinal tract, and are most commonly found in the stomach and the small intestine.[24,25] They typically originate in the muscular layer of the gastrointestinal tract and usually grows toward the lumen. At present, with the advancement of current diagnostic equipment, the possibility of early detection of GISTs has increased greatly, and the prognosis has improved.[26] However, many patients are still diagnosed with advanced disease, due to the fact that GISTs tend to be asymptomatic in the early stage.[27] Endoscopic ultrasound is a way to diagnose GISTs, but its accuracy still needs to be improved when detecting small tumors.[28] Histological examination depending on morphological features and immunohistochemical testing which is mainly based on the antibody CD117 and other markers such as DOG1 are the gold standard for the diagnosis of GISTs.[6,29] However, these diagnostic techniques are time-consuming as well as labor-intensive, and tumor biopsies may produce dissemination.[30] Therefore, it is meaningful to develop a new optical imaging technique that can match the resolution of histopathological diagnosis. MPM has excellent characteristics such as deep penetration depth, low photo-bleaching, as well as low optical damage, and is capable of label-free visualizing biological tissues at cellular and subcellular resolution,[31–34] and thus has the potential in the future to serve as an auxiliary tool for diagnosing a variety of diseases.

The change of collagen fibers often occurs with the development of tumors, and SHG imaging can precisely monitor collagen changes in the extracellular matrix such as collagen deposition. Our imaging data show that in the normal gastric muscular layer, collagen fibers are found to be striped and neatly arranged, however, collagen content obviously increases in the GISTs because of desmoplastic reaction caused by tumor invasion and these fibers are disordered. Moreover, collagen distribution in the GISTs is completely different from that in the normal mucosa and submucosa. These results suggest the utility of SHG imaging to label-free identify GISTs. By the combination of TPEF imaging, this microscope can further provide the information of cell morphology and tissue structure such as blood vessel, glands, epithelial cells, and therefore can be used to monitor precancerous lesions or tumor invavison. As reported, many

researches have been exploiting a real-time miniature endoscope for *in-vivo* experiment,[35–38] demonstrating it is feasible to develop the multiphoton endoscope. However, it still needs to develop a portable and robust ultrafast lasers, low loss laser delivery and signal collection fiber maintaining the pulse shape, compact and precise scanners as well as high-performance endomicroscopic objectives.[39]

Moreover, we use two feature descriptors, the AR and correlation, to measure the degree of collagen confusion and regularity in repetition patterns of collagen fibers. The AR increases significantly in the GISTs by comparing it with the normal gastric muscular propria because collagen fibers in GISTs are more chaotic. Statistical results also show that there is a significant difference in the AR values between the two groups. The downward trend of the correlation value for GISTs is slower than that of the normal muscular propria, possibly because of the loss of regularity in repetition patterns of collagen fibers. Quantitative results also reveal significant difference in the correlation between the two groups. Hence, combined with the quantitative analysis, SHG imaging has the potential to become an auxiliary tool in the diagnosis of GISTs. It is important to note that there are some limitations of this study: First, more samples cannot be collected to validate our results; second, the research object has *ex vivo* issues. Despite these limitations, we believe our study has demonstrated the potential use of SHG imaging for clinical practice.

## 5. Conclusions

In summary, SHG imaging is introduced to detect label-free GISTs, and the results highlight the advantages of SHG imaging in identifying GISTs. Moreover, statistical analysis shows that two feature descriptors, the AR and correlation values, can be used to quantitatively evaluate collagen changes in tumor microenvironment. With the emergence and development of multiphoton endoscopy, we have enough reason to believe that SHG imaging has the potential to become an auxillary tool in the diagnosis of GISTs in the near future.

## Acknowledgments

This project was supported by the National Natural Science Foundation of China (Grant Nos. 82171991 and 82172800), Joint Funds for the Innovation of Science and Technology of Fujian Province (Grant No. 2019Y9101), Fujian Major Scientific and Technological Special Project for "Social Development" (No. 2020YZ016002), and Special Funds of the Central Government Guiding Local Science and Technology Development (No. 2020L3008).

## Conflicts of Interest

The authors declare that they have no conflict of interest.

## References

1. A. El-Menyar *et al.*, "Diagnosis and management of gastrointestinal stromal tumors: An up-to-date literature review," *J. Cancer Res. Ther.* **13**, 889–900 (2017).
2. C. P. Raut, J. A. Morgan, S. W. Ashley, "Current issues in gastrointestinal stromal tumors: Incidence, molecular biology, and contemporary treatment of localized and advanced disease," *Curr. Opin. Gastroenterol.* **23**, 149–158 (2007).
3. L. Menon, J. M. Buscaglia, "Endoscopic approach to subepithelial lesions," *Therap. Adv. Gastroenterol.* **7**, 123–130 (2014).
4. N. Patel, B. Benipal, "Incidence of gastrointestinal stromal tumors in the United States from 2001-2015: A United States cancer statistics analysis of 50 states," *Cureus* **11**, e4120 (2019).
5. J. Tanaka *et al.*, "Small gastrointestinal stromal tumor of the stomach showing rapid growth and early metastasis to the liver," *Dig. Endosc.* **22**, 354–356 (2010).
6. M. Ceausu *et al.*, "A multidisciplinary approach in the diagnostic challenge of GIST," *Exp. Ther. Med.* **22**, 1063 (2021).
7. Y. A. DeClerck, "Desmoplasia: A response or a niche," *Cancer Discov.* **2**, 772–774 (2012).
8. O. Abbas, M. Mahalingam, "Desmoplasia: Not always a bad thing," *Histol.* **58**, 643–659 (2011).
9. P. J. Campagnola, L. M. Loew, "Second-harmonic imaging microscopy for visualizing biomolecular arrays in cells, tissues and organisms," *Nat. Biotechnol.* **21**, 1356–1360 (2003).
10. Y. Sun, H. H. Tu, S. A. Boppart, "Nonlinear optical imaging by detection with optical parametric amplification," *J. Innov. Opt. Health Sci.* **26**, 2245001 (2023).
11. R. Mouras *et al.*, "Multimodal, label-free nonlinear optical imaging for applications in biology and biomedical science," *J. Raman Spectrosc.* **44**, 1373–1378 (2013).

12. W. R. Zipfel *et al.*, "Live tissue intrinsic emission microscopy using multiphoton-excited native fluorescence and second harmonic generation," *PNAS* **100**, 7075–7080 (2003).
13. L. H. Li *et al.*, "Label-free assessment of premalignant gastric lesions using multimodal nonlinear optical microscopy," *IEEE J. Sel. Top. Quantum Electron.* **25**, 1–6 (2018).
14. Y. Zhou *et al.*, "Imaging normal and cancerous human gastric muscular layer in transverse and longitudinal sections by multiphoton microscopy," *Scanning* **38**, 357–364 (2016).
15. J. Yan *et al.*, "Real-time optical diagnosis of gastric cancer with serosal invasion using multiphoton imaging," *Sci. Rep.* **6**, 31004 (2016).
16. L. H. Li *et al.*, "Multimodal multiphoton imaging for label-free monitoring of early gastric cancer," *BMC Cancer* **19**, 295 (2019).
17. J. Adur *et al.*, "Second harmonic generation microscopy as a powerful diagnostic imaging modality for human ovarian cancer," *J. Biophoton.* **7**, 37–48 (2014).
18. S. M. Zhuo *et al.*, "Quantitatively linking collagen alteration and epithelial tumor progression by second harmonic generation microscopy," *Appl. Phys. Lett.* **9**, 213704 (2010).
19. R. M. Haraclick, K. Shanmugam, I. Dinstein, "Textural features for image classification," *IEEE Trans. Syst. Man Cybern. Syst.* **3**, 610–621 (1973).
20. R. F. Walker, P. T. Jackway, D. Longstaff, "Genetic algorithm optimization of adaptive multi-scale GLCM features," *Int. J. Pattern Recognit. Artif. Intell.* **17**, 17–39 (2003).
21. A. A. Zeitoune *et al.*, "Epithelial overian cancer diagnosis of second-harmonic generation images: A semiautomatic collagen fibers quantification protocal," *Cancer Inf.* **16**, 1176935117690162 (2017).
22. W. J. Ren *et al.*, "Visualization of lymphatic vascular invasion in breast cancer by multiphoton microscopy," *Lasers Med. Sci.* **36**, 303–309 (2021).
23. Y. Y. Hou *et al.*, "Stage and histological grade of gastrointestinal stromal tumors based on a new approach are strongly associated with clinical behaviors," *Mod. Pathol.* **22**, 556–569 (2009).
24. M. Miettinen *et al.*, "Gastrointestinal stromal tumors, intramural leiomyomas, and leiomyosarcomas in the duodenum: A clinicopathologic, immunohistochemical, and molecular genetic study of 167 cases," *Am. J. Surg. Pathol.* **27**, 625–641 (2003).
25. W. C. Foo, B. Liegl-Atzwanger, A. J. Lazar, "Pathology of gastrointestinal stromal tumors," *Clin. Med. Insights Pathol.* **5**, 23–33 (2012).
26. A. Kazuya *et al.*, "Current clinical management of gastrointestinal stromal tumor," *World J. Gastroenterol.* **24**, 2806–2817 (2014).
27. K. T. Lim, K. Y. Tan, "Current research and treatment for gastrointestinal stromal tumors," *World J. Gastroenterol.* **23**, 4856–4866 (2017).
28. T. Yoneyama *et al.*, "Diagnostic imaging of gastronintestinal stromal tumor," *Gastrointestinal Stromal Tumor*, Y. Kurokawa, Y. Komatsu (eds) (Springer, Singapore, 2019), pp. 49–59.
29. V. D. Constantin *et al.*, "A histopathological and immunohistochemical approach of surgical emergencies of GIST. An interdisciplinary study," *Rom. J. Morphol. Embryol.* **55**, 619–627 (2014).
30. K. Akahoshi *et al.*, "Preoperative diagnosis of gastrointestinal stromal tumor by endoscopic ultrasound-guided fine needle aspiration," *World J. Gastroenterol.* **13**, 2077–2082 (2007).
31. L. H. Li *et al.*, "Label-free identification of early gastrointestinal neuroendocrine tumors via biomedical multiphoton microscopy and automatic image analysis," *IEEE Access* **99**, 105681–105689 (2020).
32. L. H. Li *et al.*, "Label-free multiphoton imaging to assess neoadjuvant therapy responses in breast carcinoma," *Int. J. Biol. Sci.* **16**, 1376–1387 (2020).
33. Y. L. Liu *et al.*, "Quantitative analysis of collagen morphology in breast cancer from millimeter scale using multiphoton microscopy," *J. Innov. Opt. Health Sci.* (2023), doi: 10.1142/S17935458224 30039.
34. X. Peng *et al.*, "Observations of intracellular second-harmonic generation imaging in black phosphorus nanosheets," *J. Innov. Opt. Health Sci.* **14**, 2041006 (2021).
35. D. Y. Kim *et al.*, "Lissajous scanning two-photon endomicroscope for in vivo tissue imaging," *Sci. Rep.* **9**, 3560 (2019).
36. X. Duan *et al.*, "MEMS-based multiphoton endomicroscope for repetitive imaging of mouse colon," *Biomed. Opt. Exp.* **6**, 3074–3083 (2015).
37. W. Piyawattanametha *et al.*, "In vivo brain imaging using a portable 2.9 g two-photon microscope based on a microelectromechanical systems scanning mirror," *Opt. Lett.* **34**, 2309–2311 (2009).
38. G. Ducourthial *et al.*, "Development of a real-time flexible multiphoton microendoscope for label-free imaging in a live animal," *Sci. Rep.* **5**, 18303 (2015).
39. E. Pshenay-Severin *et al.*, "Multimodal nonlinear endomicroscopic imaging probe using a double-core double-clad fiber and focus-combining micro-optical concept," *Light Sci. Appl.* **10**, 207 (2021).